Stochastic Dynamics of El Niño–Southern Oscillation*

B. WANG

Department of Meteorology, School of Ocean and Earth Science and Technology, University of Hawaii, Honolulu, Hawaii

A. BARCILON

Department of Meteorology and GFDI, The Florida State University, Tallahassee, Florida

Z. FANG

Department of Meteorology, School of Ocean and Earth Science and Technology, University of Hawaii, Honolulu, Hawaii

(Manuscript received 21 August 1997, in final form 27 March 1998)

ABSTRACT

A stochastically forced nonlinear dynamic model for El Niño–Southern Oscillation is advanced to explore the nature of the highly irregular ENSO cycle. The model physics includes nonlinear dynamics of the coupled ocean–atmosphere system, high-frequency stochastic forcing, and the annual forcing of a prescribed climatological basic state.

The model irregular ENSO-like oscillation arises from three different origins: stochastic resonance, coupled nonlinear instability, and stochastic transition. When the basic state is stable, the stochastic forcing excites irregular oscillations by stochastic resonance. When the system is unstable and the coupled dynamics sustains a nonlinear oscillation (stable limit cycle), the stochastic forcing perturbs the deterministic trajectory of the limit cycle in the phase space, generating irregularities and modifying the oscillation period. When the system possesses multiequilibrium states, the stochastic forcing may render the system oscillatory by randomly switching the system between a warm and a cold stable steady state.

The stochastic response depends not only on the nonlinear dynamic regimes of the ENSO system but also on the temporal structure (spectrum) and strength of the stochastic forcing. White and red noises are shown to be much more effective than band-limited white noises in stochastic resonance and in altering the characteristics of the nonlinear oscillation. The intraseasonal noise can alter the dominant period of intrinsic nonlinear oscillation, favoring biennial oscillation, especially when the intraseasonal forcing is modulated by the monsoon (annual) cycle. Stronger forcing yields an enhanced resonant oscillation with a prolonged period. A sufficiently strong white noise forcing, however, can destroy the nonlinear or resonant oscillation, leading to a Markovian process. The basic-state annual variation tends to enhance the resonant oscillation but reduces the oscillation period considerably in the marginally stable regime.

The model results suggest that ENSO may arise from multimechanisms. The different mechanisms may be at work in various phases of the ENSO evolution, depending on the basic state and the nonlinear dynamics of the system. The monsoon may affect ENSO through modulation of intraseasonal stochastic forcing, enhancing the biennial component of ENSO.

1. Introduction

The evolution of ENSO exhibits conspicuous irregularities from one cycle to another. Understanding the cause of the irregularities associated with this oscillatory behavior is critical for ENSO prediction.

Recent studies with intermediate coupled models have revealed that the coupled system may display deterministic chaos due to the presence of the annual variations of the basic state upon which ENSO evolves. In models with specified seasonally varying basic states, as the dynamic coupling increases, the coupled system becomes unstable and undergoes a quasiperiodicity route to chaos due to the overlapping of the frequency-locking resonance (Tziperman et al. 1994; Jin et al. 1994). By allowing the annual cycle to interact with the ENSO cycle, Chang et al. (1994) demonstrate that as

* School of Ocean and Earth Science and Technology Publication Number 4076, and GFDI Publication Number 400.

Corresponding author address: Dr. Bin Wang, Department of Meteorology, University of Hawaii, 2525 Correa Rd., Honolulu, HI 96822.

the external annual heat flux forcing strengthens, the coupled system experiences a number of transitions between periodic and chaotic oscillations. The system finally gives up its intrinsic ENSO oscillation and acquires the oscillation period of the external annual forcing. The deterministic chaos found in these intermediate coupled models is characteristic of low-order dynamic systems (Tziperman et al. 1995; Chang et al. 1995).

However, the irregular interannual oscillation simulated by coupled general circulation models (CGCMs) (Philander et al. 1992) does not appear to be of the low-order chaos. The nonlinear time series analysis performed by Chang et al. (1996) suggests that stochastic processes, rather than chaotic dynamics, are likely to be a major source of ENSO irregularity in CGCMs and in nature. This implies that high-frequency processes may play a critical role in the ENSO evolution (e.g., Graham and White 1988; Kleeman and Power 1994). It has been suggested that ENSO is a manifestation of a stochastically driven oscillation (e.g., Lau 1985; Penland and Matrosova 1994; Penland and Sardeshmukh 1995; Penland 1996; Eckert and Latif 1997; Blanke et al. 1997). The causes of the irregular ENSO cycles remain inconclusive. The roles of the nonlinear chaotic dynamics and of the stochastic forcing in the ENSO evolution and in limiting the ENSO predictability invite further investigations.

The tropical ocean–atmosphere climate system may be considered as a nonlinear coupled system influenced by high-frequency (synoptic to intraseasonal) forcing and exhibits low-frequency (interannual) variations. The high-frequency forcing has much shorter characteristic timescales compared to ENSO and may be treated as stochastic. The coupled system also experiences a prescribed annual forcing (via change of the mean state upon which ENSO evolves). Our interests focus on the roles of the stochastic forcing and the coupled nonlinear dynamic regimes in generating and sustaining highly irregular ENSO cycles. A number of critical questions need to be addressed:

(i) How does the response of the ENSO system to stochastic forcing (hereafter the stochastic response) relate to the nonlinear dynamics of the coupled system? The answer to this question will help clarify the relative roles played by the nonlinear dynamics and the stochastic forcing in the ENSO evolution.

(ii) How does the stochastic response depend on the temporal structure and intensity of the stochastic forcing? In general, the stochastic response depends on both the spatial and temporal characteristics of the stochastic forcing. Recent studies have focused on searching for spatial patterns of the stochastic forcing (stochastic optimal) that enhance low-frequency variability of the coupled system (e.g., Kleeman and Moore 1997), whereas far less attention has been given to the investigation of the impacts of the temporal structure of the stochastic forcing on the low-frequency variability of the coupled system.

(iii) What roles does the basic-state annual cycle play in the stochastic dynamics of the ENSO system? What are the differences between linear and nonlinear stochastic responses?

To address these questions, we adopt the nonlinear dynamics system model for ENSO advanced by Wang and Fang (1996, hereafter WF96) and extend the model to include stochastic forcing. Section 2 and appendix A describe the model physics and its formulation. Section 3 discusses the deterministic dynamics of the ENSO model without stochastic forcing. Although highly idealized, it will be shown that the model contains the essential dynamics relevant to capture the observed ENSO evolution and the interannual oscillations found in intermediate coupled models and CGCMs. This then is one of the reasons for choosing this theoretical model. In addition, because of its computational efficiency, this model enables us to carry out a large number of numerical experiments, which would be prohibitive in coupled GCMs. The results derived from this simple model are expected to provide physical insight to help interpret the results obtained from more complex coupled models. In sections 4, 5, and 6, we address the three questions raised in the previous paragraph. The last section presents a summary of this work.

2. The stochastic dynamics model for ENSO: Formulation

With a number of simplifications, WF96 distilled Zebiak and Cane's (1987) intermediate coupled ocean–atmosphere model to a theoretical model, which is referred to as the ENSO system hereafter. The ENSO system consists of only two prognostic equations: one describing the oceanic mixed layer thermodynamics and the other depicting the upper-ocean dynamics [see appendix A, Eqs. (A1), (A2)]. The atmosphere serves as a medium through which SST anomalies affect ocean dynamics [Eq. (A3)].

To the lowest-order approximation, the spatial structure of ENSO is characterized by an equatorial symmetric, east–west standing oscillation. Such a seesaw oscillation is obvious in SST and sea level pressure fields (e.g., Trenberth and Shea 1987). The thermocline variation, which ''memorizes'' the aftermath of the SST on the surface winds and conveys wind feedback to the SST, also features a basinwide seesaw oscillation: The thermocline displacements represented by the depth of the 20°C isotherm and averaged over the western (120°E–160°W) and eastern (160°–80°W) basins between 15°S and 15°N and between 25°S and 25°N are all nearly 180° out of phase (Fig. 1). This east–west seesaw structure is consistent with the theory of Cane and Moore (1981), who showed that the thermocline adjustment in a zonally bounded basin results in a low-frequency standing basin mode. In the coupled model

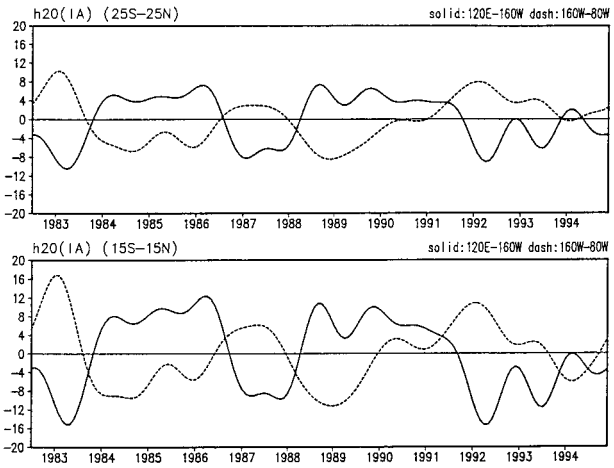

FIG. 1. Monthly mean anomalies of the 20°C isotherm depth averaged over the western (west of 160°W) and the eastern (east of 160°W) Pacific basin (a) between 25°S and 25°N, and (b) between 15°S and 15°N. The anomalies are 11-month running means. The original data are derived from the Ocean Data Assimilation System at the National Centers for Environmental Prediction (Ji et al. 1995).

of Zebiak and Cane (1987), Wakata and Sarachik (1991) showed that the unstable coupled basin anomaly mode in a spatially varying basic state exhibits a similar structure: The thermocline fluctuation in the western and eastern section of the basin tends to be out of phase, while sharp phase changes concentrate in the central equatorial Pacific.

The equatorial symmetric, east–west seesaw structure of the coupled mode provides a physical basis for further simplification of the ENSO system by use of Lorenz's (1963) spectral truncation approach (appendix A). Then, the temporal structure of the standing ENSO mode may be described by a second-order nonlinear dynamic system with periodic coefficients describing the annual variation of the basic state (WF96).

Appendix A extends the WF96 model by incorporating high-frequency, unresolved physical processes, which we treat as stochastic forcing. The justification for such a treatment may be found in, say, Penland and Sardeshmukh (1995). The resultant nondimensional governing equations for the anomalous SST, T, and thermocline depth, h, averaged over the equatorial eastern Pacific and projected onto the lowest meridional structure mode are [Eqs. (A7) and (A8)]

$$\frac{dT}{dt} = a_1 T + a_2 h + a_3 T(T - \mu h) - 2T^3 + \mathrm{SF}_1, \tag{2.1a}$$

$$\frac{dh}{dt} = b(2h - T) - 2h^3 + \mathrm{SF}_2, \tag{2.1b}$$

where

$$a_1 = \Delta\overline{T}'_z + \Delta\overline{T}'_x - \alpha'_s, \tag{2.2a}$$

$$a_2 = -\mu\Delta\overline{T}'_x, \tag{2.2b}$$

$$a_3 = \sqrt{\frac{2}{3}}, \tag{2.2c}$$

$$b = \frac{2\alpha}{p(1 - 3\alpha^2)}, \tag{2.2d}$$

$$\mathrm{SF}_1 = \Delta\overline{T}'_z u^s, \tag{2.2e}$$

$$\mathrm{SF}_2 = -3bu^s. \tag{2.2f}$$

The coefficients a_1 and a_2 involve nondimensional basic-state parameters ($\Delta\overline{T}'_z$ and $\Delta\overline{T}'_x$) and α'_s whose meaning and corresponding dimensional values are given in Table 1. The coefficient μ measures the effect of the thermocline displacement on SST. The nondimensional parameter b is a function of the air–sea coupling coefficient α, and the model parameters $p = (1 - H_1/H)(L_0/L_s)^2$ (symbols contained in the expression for p are defined in Table 1). The parameter b represents the collective effects of the equatorial Kelvin and Rossby waves in adjusting the thermocline (WF96). Typical values for the model nondimensional coefficients and parameters are presented in Table 2.

The air–sea coupling coefficient,

$$\alpha = \left(\frac{L_0}{L_y}\right)^2, \tag{2.2g}$$

TABLE 1. List of the model parameters.

L	Zonal width of the ocean basin	1.7×10^7 m
H	Mean depth of the thermocline	150 m
H_1	Depth of the mixed layer	50 m
d	Nondimensional atmospheric boundary layer depth	0.2
$1 = \rho_a C_D/\rho_0 H$	Wind stress coefficient	10^{-8} m^{-1}
a_s	Newtonian cooling coefficient for SST anomaly	(125 day)$^{-1}$
r_s	Rayleigh friction coefficient in the oceanic mixed layer	(1.5 day)$^{-1}$
r_a	Rayleigh friction coefficient in atmospheric boundary layer	3.6×10^{-6} s^{-1}
C_0	Oceanic Kelvin wave speed	2.0 m s^{-1}
L_0	Oceanic Rossby radius of deformation	300 km
$L_s = r_s/\beta$	Ekman spreading length scale	338 km
$\Delta\overline{T}_x = \overline{T}_e - \overline{T}_w$	Mean temperature difference between the east and west	−3.5°C
$\Delta\overline{T}_z = \overline{T} - \overline{T}_e$	Mean vertical temperature difference at mixed layer base	3.0°C

TABLE 2. Typical values of the model nondimensional coefficients and parameters in the ENSO system (2.1).

a_1	a_2	μ	α	b
−0.97	−2.84	1.7	0.14	0.58

is the square of the ratio of the oceanic Rossby radius of deformation, L_0, to the characteristic meridional length scale of the coupled ENSO mode, L_y. WF96 showed that α also measures the strength of the equatorial current response to a given wind stress, and thus measures the degree of the air–sea coupling. The Pacific Ocean basin geometry provides a natural zonal scale for ENSO. The dynamical effect of the equator, that is, the change of sign in the Coriolis parameter, determines the meridionally trapped scale at the equator, the Rossby radius of deformation. It is about 300 km for the ocean and 1500 km for the atmosphere (for the lowest internal vertical mode). For the coupled ENSO mode, the meridional scale must be in between these two values, but it may vary. We treat the meridional scale of the ENSO mode as a free parameter and use it to measure the degree of the air–sea coupling. When the meridional length scale of the coupled ENSO mode varies from 1000 km to 500 km, the corresponding air–sea coupling coefficient α increases from 0.09 to 0.36 and the corresponding parameter b increases from 0.35 to 2.2.

The terms SF_1 and SF_2 represent model stochastic forcing due to atmospheric high-frequency surface zonal wind variability. The effects of stochastic variations in surface heat flux and the high-frequency oceanic processes are neglected. Over the Pacific, especially over the warm pool region, there is a large variance on synoptic to intraseasonal timescales. Although the behavior of intraseasonal oscillations is affected by ENSO, for simplicity, we consider that this intraseasonal ''noise'' is not directly coupled with the SST variation on the ENSO timescale, but may have a potential influence on ENSO by exciting low-frequency perturbations in the coupled system. Note also that the terms SF_1 and SF_2 represent the projection of the ''real'' stochastic forcing onto the spatial structure of the standing ENSO mode in the present highly truncated dynamic system model.

For convenience, we hereafter simply refer to Eqs. (2.1a,b) as the ENSO system. This system describes the temporal evolution of the equatorial eastern Pacific SST and thermocline depth anomalies associated with the basinwide standing mode. The first equation, (2.1a), depicts mixed layer thermodynamics that governs the SST variation in the equatorial eastern Pacific. These processes include the vertical advection of heat by mean upwelling acting on anomalous vertical temperature gradients and by anomalous upwelling acting on the mean vertical temperature gradients, the horizontal advection of heat by mean zonal currents, and thermal damping representing all processes that relax SST back to its climatology. The second equation, (2.1b), depicts the upper-ocean dynamics associated with the basinwide standing mode. The local thermocline displacement is determined by the equatorial zonal wind stress and is adjusted by the remotely forced equatorial Kelvin and Rossby waves. The collective effects of these equatorial waves result in a basinwide thermocline adjustment and provide eventually a delayed change of the thermocline depth in the equatorial eastern Pacific. For detailed model physics the readers are referred to WF96 and appendix A. Two cubic damping terms have been added to the SST and thermocline equations of WF96 to mimic, respectively, the missing nonlinear effects in the upper-ocean dynamics (Münnich et al. 1991) and the nonlinear influence of the thermocline displacement on SST variation (Battisti and Hirst 1989). In the absence of the stochastic forcing, numerical experiments show that the nonlinear oscillation (limit cycle) of the ENSO system is not qualitatively affected by adding these terms, but the parameter domain within which the limit cycle exists is substantially enlarged by the addition of these cubic nonlinear terms, which stabilize the nonlinear system. The effects of the increased degree of nonlinearity will be discussed in detail in section 7.

3. Deterministic coupled dynamics of the ENSO system

In the absence of stochastic forcing, the existence of the model interannual oscillation does not depend on whether there is a basic-state annual cycle. For simplicity, we assume that the basic state is the time-independent climatological mean state. A dynamic-regime diagram for the ENSO system in the parameter plane of the air–sea coupling coefficient α and the thermocline effect coefficient μ is shown in Fig. 2. The regimes are obtained by examining equilibrium solutions that identify the region of multiequilibria and by studying the stability of the single equilibrium state—the climatological mean state, which distinguishes the damped and limit-cycle regimes. In the α–μ plane we will use α as the bifurcation parameter while fixed $\mu = 1.7$ (in dimensional value this means that when thermocline rises 10 m the subsurface temperature T_e decreases by 0.7°C).

In the stable regime, where the coupling coefficient α is smaller than a critical value α_0 and the thermocline effect coefficient μ is sufficiently large (greater than $\mu_0 = 1.3$), the system has only one stable steady state: the climatological mean state. Any perturbation undergoes a decaying oscillation and finally approaches this climatological mean state. No sustained oscillation is possible.

When the air–sea coupling coefficient α exceeds the bifurcation point α_0, the climatological mean state becomes unstable and the coupled system evolves into a limit cycle regime. Perturbations away from the climatological mean state experience a growing oscillation and finally approach a finite-amplitude interannual oscillation (Fig. 3a). This steady nonlinear oscillation is

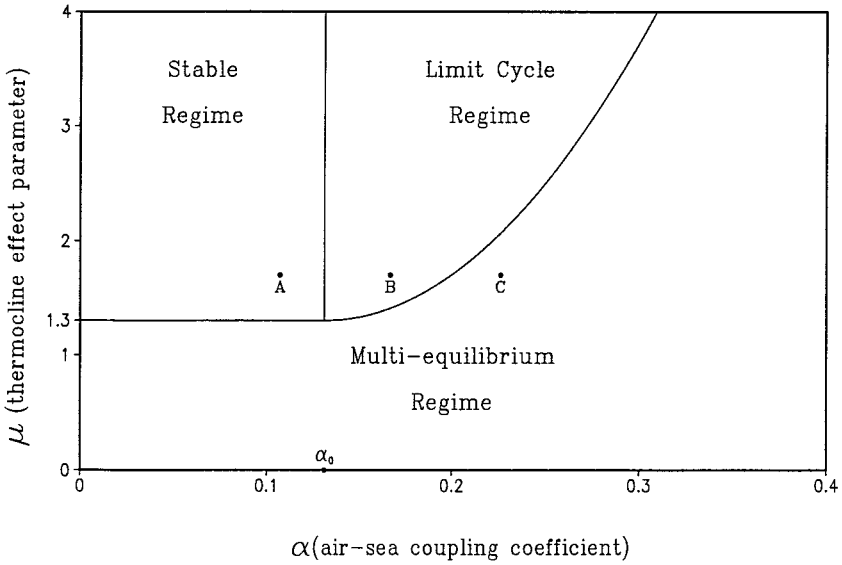

FIG. 2. Nonlinear dynamic regime diagram for the ENSO system (2.1a,b) with an annual mean basic state. The selected points *A*, *B*, and *C* represent, respectively, the stable, the limit cycle, and the multiequilibrium regime. α_0 denotes the bifurcation value at which the coupled system changes from the stable to limit cycle regime.

represented by a unique limit cycle solution in the phase plane, which acts as an attractor. As shown in WF96, the limit cycle oscillation is characterized by a moderate lead of the thermocline displacement to the SST variation, similar to the observed ENSO cycle and to the interannual variations simulated by CGCMs (e.g., Philander et al. 1992) and coupled intermediate models (e.g., Zebiak and Cane 1987).

As the bifurcation parameter α further increases, the coupled system enters a new multiequilibrium regime. There exist two stable nodes (one representing a warm state and the other representing a cold state) and two unstable saddle points in addition to the unstable climatological mean state (unstable center). In this regime, deviations away from the climatological mean state will be attracted to one of the two stable equilibrium states; no sustained oscillation is possible.

The intrinsic oscillation in the limit cycle regime results from the interaction between the surface winds and SST via nonlinear temperature advection associated with the equatorial upwelling and thermocline variation. As illustrated in Fig. 4, this nonlinear interaction involves both a positive and a negative feedback. The positive feedback arises from the chain reaction among the SST gradient, the Walker circulation, and the equatorial upwelling. Assume that a positive SST anomaly occurs in the equatorial eastern Pacific. This will reduce the zonal SST gradient along the equator and weaken the climatological mean easterlies to the west of the SST anomaly. The weakening of the easterlies reduces equatorward Ekman convergence in the surface layer and suppresses the mean equatorial upwelling, leading to further warming in the eastern Pacific. This positive feedback was first visualized by Bjerknes (1969) and demonstrated by previous coupled stability analyses (e.g., Philander et al. 1984; Hirst 1986; Neelin 1991). This instability is a major cause of the rapid warming. It depends on the mean upwelling and the large mean vertical temperature difference between the mixed layer and entrained water, $\Delta\overline{T}'_z$, in the eastern Pacific.

The negative feedback involves two processes: the vertical advection of heat by mean upwelling and the vertical displacement of thermocline due to ocean wave adjustment. When the warming in the eastern Pacific is sufficiently strong, the above two processes act against the warming. First, the warming increases anomalous vertical temperature difference across the mixed layer base, $T - T_e = T - \mu h$ (where T_e denotes the entrained water temperature from beneath the mixed layer). When $T - T_e$ is greater than normal, the vertical advection induced by the mean upwelling would suppress the warming. Second, when the warming is sufficiently strong so that $T > 2h$ (nondimensional), the thermocline depth in the equatorial eastern Pacific will decrease if b is positive [see Eq. (2.1b)]. The rising thermocline would lower the temperature of the water upwelled into the mixed layer and suppress warming. The rising of the thermocline in the eastern Pacific results from basinwide thermocline adjustment due to the collective effects of the equatorial Kelvin and Rossby waves. A positive b means that the off-equatorial Rossby waves play a dominant role in the basinwide thermocline adjustment (WF 96). Therefore, the rise of the thermocline in the eastern Pacific acts together with the mean upwelling effect to provide a negative feedback mecha-

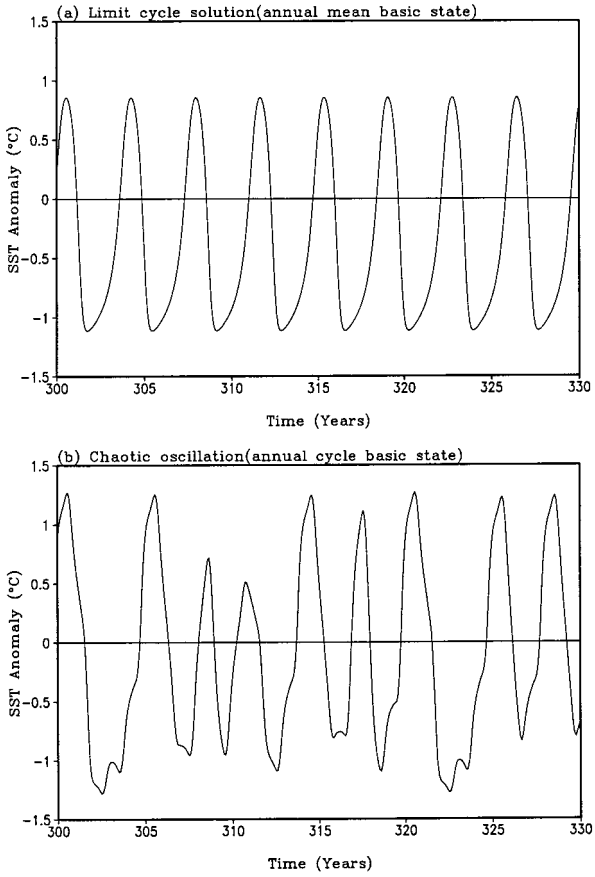

FIG. 3. Anomalous SST time series corresponding to (a) a limit cycle solution in the presence of annual-mean basic state and (b) a chaotic oscillation in the presence of annually varying basic state. No stochastic forcing is involved.

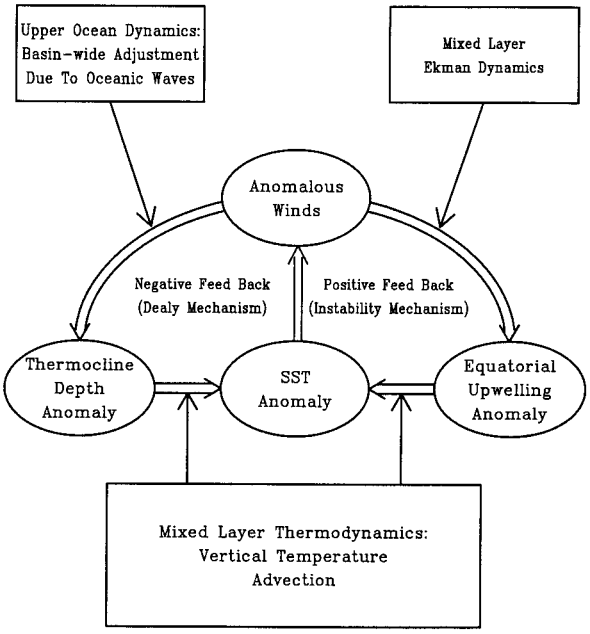

FIG. 4. Schematic diagram showing the oscillation mechanism of the ENSO system described by Eqs. (2.1a) and (2.1b).

nism against the warming and to reverse the system to a cooling stage.

The notion of the basinwide thermocline adjustment includes the collective effects of the Kelvin and Rossby waves, which are key players in the delayed oscillator idea put forth by McCreary (1983), Suarez and Schopf (1988), Battisti and Hirst (1989), and Cane et al. (1990). However, the present theory differs from the delayed action oscillator theory in the following aspects: (i) The nonlinear vertical temperature advection is essential (without this nonlinearity, the limit cycle does not exist), whereas the delayed oscillation can be reproduced without considering detailed thermodynamics (Cane et al. 1990); (ii) the basinwide thermocline adjustment is not only attributed to the equatorial waves but also to the local wind-induced Ekman pumping, the latter being a coupled process; and (iii) the timescale of the oscillation is not directly related to the timescales for the equatorial Kelvin wave and the equatorially trapped Rossby waves across the basin. The oscillation period in the present model is determined by the basinwide thermocline adjustment (within the meridional scale of the coupled mode) and a time interval needed for the upwelling to affect SST; thus it depends on the thermocline effect coefficient μ. The basinwide thermocline adjustment in the tropical Pacific is a slow process, normally taking more than a year, depending on the meridional scale of the coupled mode. When the meridional scale increases, more Rossby waves with less trapped meridional structure contribute to the basinwide thermocline adjustment. Because these less trapped meridional modes propagate slower, the adjustment time becomes longer and so does the oscillation period. This model result is consistent with the results derived from a coupled numerical model by Kirtman (1996).

Although the model intrinsic oscillation does not depend on the basic-state annual cycle, the latter has a fundamental impact on the ENSO cycle. On one hand, it makes the ENSO cycle phase-lock to the annual cycle; on the other hand, it transforms the limit cycle to a strange attractor and makes the oscillation chaotic (Fig. 3b). The latter behavior is very similar to and consistent with the results obtained from coupled intermediate models (Tziperman et al. 1994; Jin et al. 1994; Chang et al. 1994).

4. Dependence of the stochastic response on the coupled dynamics

In the presence of stochastic forcing, the response of the ENSO system depends critically on the dynamic regimes of the system. To demonstrate how the stochastic response of the ENSO system depends on the nonlinear dynamics of the coupled system and to avoid complication, we assume that (i) the basic state is time independent (the climatological mean state) and (ii) the

stochastic wind forcing is a white noise with a moderate amplitude (standard deviation is 1.17 m s^{-1}). The effects of changes in the characteristics of the stochastic forcing and the impacts of the annual variation of the basic state will be discussed in the next two sections, respectively. The representative parameter values (α and μ) for different dynamic regimes are illustrated in Fig. 2 by points A, B, and C.

Even if one fixes the type of stochastic forcing (such as a white noise), an infinite number of possible realizations of the white noise process may exist. The response time series would differ in the details for different individual realizations of the stochastic forcing. However, our numerical experiments have shown that the resultant response spectra (i.e., the spectrum derived from the response time series) do not exhibit statistically significant differences. One can, therefore, faithfully describe the stochastic response of the ENSO system using its response spectrum.

a. Stochastic resonance in the stable regime

When $\alpha = 0.11$ and $\mu = 1.7$ (point A in Fig. 2), the climatological mean state is a stable steady state. There is no sustained intrinsic oscillation without stochastic forcing. However, when a white noise is introduced into such a stable ENSO system, the system displays sustained irregular oscillations as shown in Fig. 5a. The spectrum of the corresponding time series shows a broad peak centered around 3 yr (the thick solid line in Fig. 5d). The concentration of energy on the interannual timescale indicates that the white noise excites and sustains a low-frequency irregular oscillation. The dominant period is that of the intrinsic damped oscillation of the system. This provides an example of a resonant response of a dynamic system to an external stochastic forcing, which does not depend on the internal dynamic instability of the coupled system.

We assume that the dynamics near the stable attractor, which represents the mean climate state, is linear. This implies that the stochastic excursions away from the climatic state are not too large. In this case, the linear dynamics amounts to that of a linear damped and stochastically forced pendulum. The evolution equation for that system is described by an Ornstein–Uhlenbeck process (Gardiner 1983):

$$d\mathbf{x}(t) = \mathbf{B}\, dt + \mathbf{D}\, dW(t), \tag{4.1}$$

where the $\mathbf{x}(t) = (T, h)^{\mathrm{T}}$ denotes a state vector whose components are anomalous temperature and thermocline depth. The constant matrix $\mathbf{B}$ is expressed in terms of the constant coefficients of the ENSO system [see (2.1)] as

$$\mathbf{B} = \begin{pmatrix} a_1 & a_2 \\ -b & 2b \end{pmatrix}. \tag{4.2}$$

In the damped oscillatory region the eigenvalues of $\mathbf{B}$, $\beta_{1,2}$, have a negative real part $\gamma = (2b + a_1)/2$ and are given as

$$\beta_{1,2} = -\gamma \pm \sqrt{\gamma^2 - b(2a_1 - a_2)}. \tag{4.3}$$

At point A in Fig. 2, the numerical values of these eigenvalues are $\beta_{1,2} \equiv -\gamma \pm i\omega_0 = -0.073 + i0.609$, showing that the ratio of the damping term to the frequency term is about one-tenth. In the last term in (4.1), $dW(t)$ can be thought of as being the product $\xi\, dt$ where ξ represents a white noise; the constant matrix $\mathbf{D}$ is associated with the amplitudes of the stochastic forcing in the (T, h)-differential equations and may be denoted as

$$\mathbf{D} = \mathbf{C}_1 \begin{pmatrix} 1 & 0 \\ 0 & \delta \end{pmatrix}, \tag{4.4}$$

where $\mathbf{C}_1$ and $\delta\mathbf{C}_1$ are amplitudes of the stochastic forcing. Focusing on the stationary solution, $\mathbf{x}_s(t)$, of (4.1) (Gardiner 1983), we find

$$x_s(t) = \int_0^t \exp[\mathbf{B}(t - t')]\mathbf{D}\, dW(t'). \tag{4.5}$$

The amplitude of the stochastic forcing, represented by $\mathbf{D}$, must affect the amplitude of the motion, which can be represented by the covariance matrix

$$\sigma = \langle \mathbf{x}_s(t), \mathbf{x}_s^{\mathrm{T}}(t) \rangle. \tag{4.6}$$

In the above expressions, $\langle\ ,\ \rangle$ denotes expectation values and $(\ )^{\mathrm{T}}$ denotes the transpose of a vector. For a stationary process, the fluctuation–dissipation relation

$$\mathbf{B}\sigma + \sigma\mathbf{B}^{\mathrm{T}} + \mathbf{D}\mathbf{D}^{\mathrm{T}} = 0, \tag{4.7}$$

ties the amplitude of the dynamics to that of the stochastic forcing (Gardiner 1983; Farrell and Ioannou 1996; Penland 1996). The matrix $\mathbf{B}$ is intimately connected to the propagator or Green's function, $G_s(\tau)$ since

$$G_s(\tau) = \exp[\mathbf{B}\tau], \tag{4.8}$$

and the state vector at time τ relates to the state vector at time zero as

$$\mathbf{x}(t) = \exp[\mathbf{B}\tau]\mathbf{x}(0), \tag{4.9}$$

a relation used by Penland and collaborators (Penland and Matrosova 1994; Penland 1996; Penland and Sardeshmukh 1995) to obtain ENSO forecast once $\mathbf{B}$ is obtained from SST data.

Finally, following Gardiner (1983), we can construct the spectrum matrix as

$$\mathbf{S}(\omega) = \frac{1}{2\pi}(\mathbf{B} + \mathbf{I}\omega\mathbf{I})^{-1}\mathbf{D}\mathbf{D}^{\mathrm{T}}(\mathbf{B}^{\mathrm{T}} - \mathbf{I}\omega\mathbf{I})^{-1}, \tag{4.10}$$

where $\mathbf{I}$ is the unit matrix. The (1, 1) element of $\mathbf{S}(\omega)$ provides the spectral power of the SST anomalies as a function of ω, the frequency, and is given as

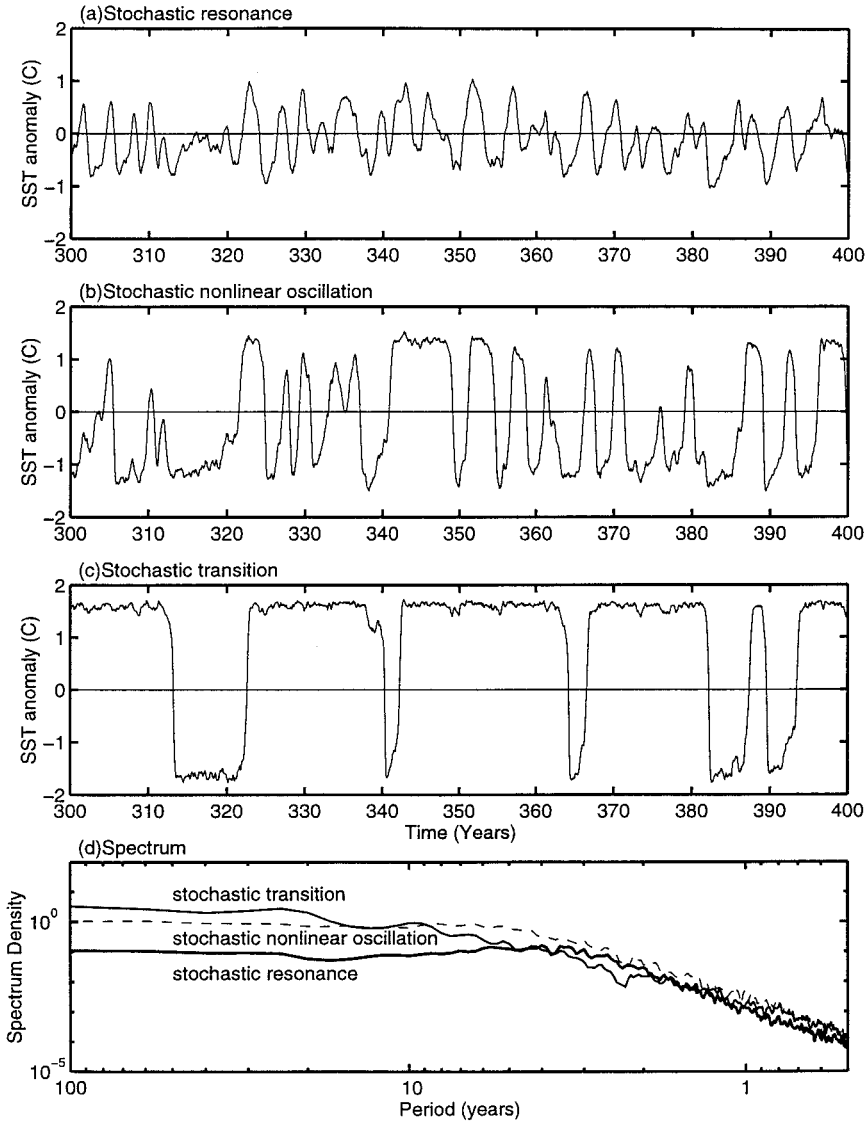

FIG. 5. The anomalous SST time series derived from the stochastic response of the ENSO system (2.1) to a white noise forcing in (a) the stable regime (point A in Fig. 2), (b) the limit cycle regime (point B in Fig. 2), and (c) the multiequilibrium regime (point C in Fig. 2). The corresponding response spectra for (a), (b), and (c) are shown in (d) by thick solid, dashed, and thin solid lines, respectively. No basic-state annual cycle is considered. The standard deviation of the white noise forcing is 1.17 m s^{-1}.

$$S_{1,1} = \frac{C_1^2(\delta^2 + 4\delta\gamma + 4\gamma^2 + \omega^2)}{2\pi[(\omega_0^2 - \omega^2)^2 + 2\gamma^2(\omega_0^2 + \omega^2) + \gamma^4]}, \tag{4.11}$$

where ω_0 is the intrinsic frequency of the damped oscillation. A plot of $S_{1,1}/C_1^2$ (not shown) shows that there is a stochastic resonance at

$$\omega^2 \cong \omega_0^2 + \left(\frac{\omega_0^2 - \delta^2}{\omega_0^2 + \delta^2}\right)\gamma^2 = \omega_0^2 + O(\gamma^2), \tag{4.12}$$

that is, not very far from ω_0^2.

b. Stochastic nonlinear oscillation in the limit cycle regime

When $\alpha = 0.17$ and $\mu = 1.7$ (the point B in Fig. 2), the climatological mean state is unstable and the ENSO system possesses a unique limit cycle solution—a perpetual regular oscillation. When stochastic forcing is included, the nonlinear oscillation becomes irregular as shown in Fig. 5b. The original spectrum peak located at about 3 yr is smeared. The corresponding energy spreads over adjacent frequencies (the dashed line in Fig. 5d). Meanwhile the energy level at all frequencies is raised. The irregularity of the oscillation is not due

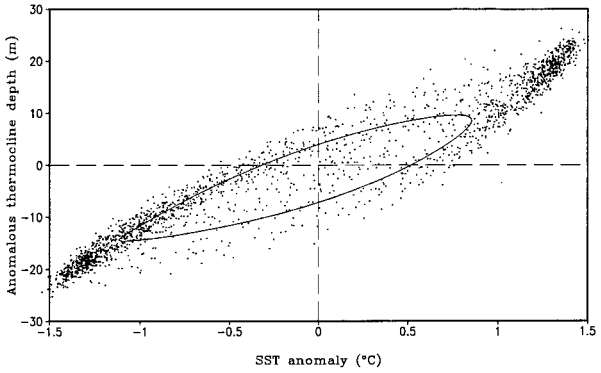

FIG. 6. The phase orbit of the limit cycle without stochastic forcing (solid curve) and the phase-scattering diagram showing the stochastic response of the ENSO system in the same limit cycle regime (point B in Fig. 2).

to low-order deterministic chaos because the mechanism responsible for the chaos, the annual cycle of the basic state, is absent. In this case, the oscillation originates from the nonlinear dynamics of the ENSO system, but the white noise forcing makes it irregular. The presence of a white noise forcing disperses energy from the intrinsic oscillation period to shorter and longer timescales.

In the phase plane, the stochastic forcing perturbs the phase trajectory representing the regular limit cycle (Fig. 6). The resultant trajectory tends to spread around the limit cycle and, in particular, to densely populate in the neighborhood where the tendencies of the deterministic solutions are small. The latter feature corresponds to the presence of occasionally prolonged warming or cooling episodes in the response time series shown in Fig. 5b. The stochastic perturbation is also responsible for the dispersion of the major spectral peak in the response spectrum shown in Fig. 5d.

For small stochastic forcing, we may write (4.1) in a vector form as

$$d\mathbf{x} = \mathbf{F}(x)\, dt + \epsilon \mathbf{D}\, dW(t),$$

where $\mathbf{x}$ is a two-dimensional state vector, $\mathbf{F}(x)$ is a vector consisting of the deterministic nonlinear dynamics on the right-hand side of (2.1), and $\epsilon\mathbf{D}$ is a constant 2×2 matrix characterizing the nondimensional amplitude of the stochastic forcing. Figure 6 shows a pronounced clustering of points when the deterministic solution is nearly stationary. Therefore, assuming $\epsilon \ll 1$, we write

$$x = x_0 + \epsilon x_1(t) + \cdots,$$

$$\mathbf{F}(x) = \mathbf{F}(x_0) + \epsilon\left(\frac{\partial \mathbf{F}}{\partial x}\right)_0 x_1 + \cdots,$$

where $(\partial \mathbf{F}/\partial x)_0$ is the Jacobian derivative

$$\begin{pmatrix} \dfrac{\partial F_1}{\partial T} & \dfrac{\partial F_1}{\partial h} \\ \dfrac{\partial F_2}{\partial T} & \dfrac{\partial F_2}{\partial h} \end{pmatrix}$$

evaluated at x_0, which we will assume stationary. Then the $O(\epsilon)$ dynamics is described by an Ornstein–Uhlenbeck process (Gardiner 1983) governed by

$$dx_1 = \left(\frac{\partial F}{\partial x}\right)_0 x_1 dt + \mathbf{D} dW(t), \tag{4.13}$$

whose solution is

$$x_1(t) = \int_0^t \exp\left[\left(\frac{\partial F}{\partial x}\right)_0 (t - t')\right]\mathbf{D}\, dW(t'), \tag{4.14}$$

where we have taken $x_1(0) = 0$. Then, in some approximate sense, the two neighborhoods of the turning points of the deterministic solution behave as quasi-stationary points as can be seen by comparing (4.14) with (4.5).

c. *Stochastic transition in the multiequilibrium regime*

When $\alpha = 0.23$ and $\mu = 1.7$ (point C in Fig. 2), the ENSO system possesses two stable equilibrium states (Fig. 7): a warm state (WS) and a cold state (CS), which may represent El Niño and La Niña, respectively. In addition, three unstable steady states exist: the climatological mean state (the center CM) and two saddles U_1 and U_2. The spiral line across the three unstable states divides the entire plane into two attraction basins. The above equilibrium states and the attraction domains are obtained by searching for steady solutions of (2.1) and by studying the stability of each equilibrium state analytically and by means of numerical integration. In the absence of stochastic forcing, any initial perturbation located in the lower attraction basin (the cold attraction basin) will approach CS, whereas those located in the upper attraction basin (the warm attraction basin) will be attracted to WS.

The presence of a white noise forcing constantly perturbs the ENSO system away from the two stable equilibrium states. Although the warm equilibrium state is located within the warm attraction basin, under certain conditions, the stochastic perturbation can be sufficiently strong to push the system into the cold attraction basin where the system will be attracted to the opposite equilibrium state.

The deterministic nonlinear dynamics establishes the basins of attraction as well as the distance between adjacent pairs of saddle nodes. This distance in phase space establishes the depth of the ''potential wells'' associated with the warm/cold steady states. The stochastic forcing must then produce motions of sufficient intensity so that the representative points in the phase

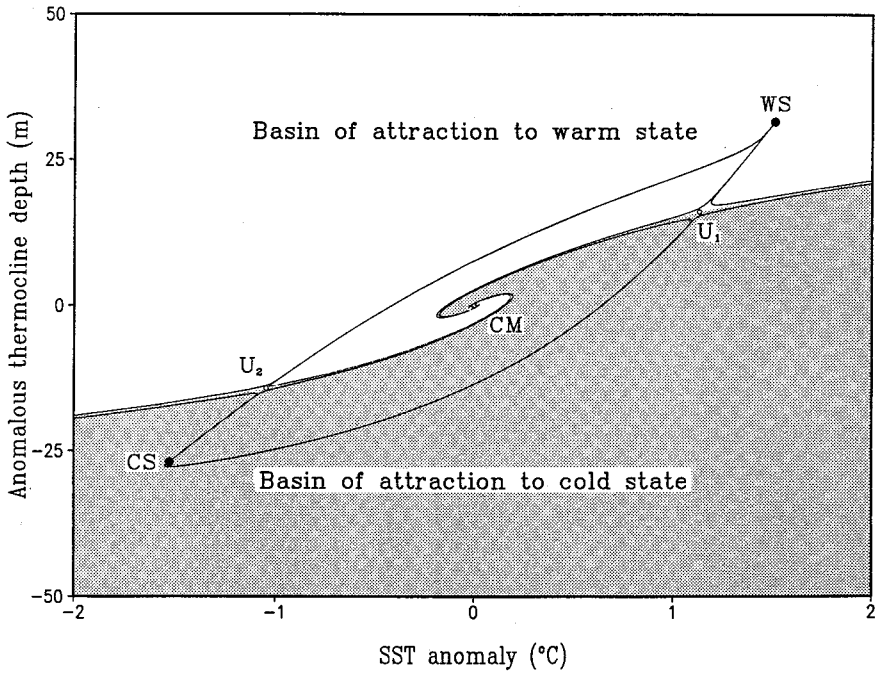

FIG. 7. Steady states of the ENSO system (2.1) in the multiequilibrium regime (point C in Fig. 2). The open circles CM, U_1, and U_2 represent, respectively, the unstable climatological mean state (CM) and two unstable saddle points (U_1 and U_2). The solid circles WS and CS denote the warm and cold stable equilibrium states (two stable nodes), respectively. The shading (blank) area represents the attraction domain of the cold (warm) steady state.

space be repelled by the saddles from one attractor basin to the other.

This leads to an oscillatory switching between the two stable states (Fig. 5c). The period of the ''switch'' oscillation is dictated by the frequency of the transition, which depends on a number of factors, mainly the intensity of the stochastic forcing, the basic-state, and coupling parameters, which control the relative locations of the steady states in their corresponding attraction basins. The stronger the stochastic forcing and the closer the steady state is to the boundary of the attraction basin, the easier for the transition to occur. This switching oscillation can occur on interannual timescales (figure not shown).

5. Dependence of the stochastic response on the properties of the forcing

In addition to the coupled dynamics, the characteristics of the stochastic forcing strongly affect the stochastic response of the ENSO system. In this section, we assess the roles of stochastic forcing in the absence of deterministic chaos, that is, by using a climatological annual mean basic state.

a. Dependence on noise levels

Figure 8 illustrates how the ENSO system responds to the intensity (or level) of a white noise forcing. The intensity of the noise is estimated by the sample standard deviation of the noisy surface zonal wind speed (m s^{-1}). In the stable regime (Fig. 8a), a stronger white noise results in a larger amplitude of the resonant oscillation. This is evidenced by the increased energy at the major spectral peak in spite of the fact that peak becomes less sharp. Furthermore, the primary oscillation period increases slightly with increasing noise level. When the noise level is sufficiently high, the evolution tends to approach a red response spectrum.

In the limit cycle regime (Fig. 8b), an increase in the noise level leads to (i) a weakening of the intrinsic oscillation as evidenced by the decrease of the primary spectral peak, (ii) an increase in irregularity as implied by the broadening of the primary spectral peak, and (iii) an increase in the oscillation period. For sufficiently strong white noise forcing, the stochastic response tends to be similar, irrespective of the dynamic regimes of the coupled system. In that case, either the stochastic nonlinear oscillation in the limit cycle regime or the resonant oscillation in the stable regime attains a similar degree of irregularity and possesses a spectrum similar to that of a Markovian process.

b. Dependence on noise spectra

Atmospheric disturbances tend to occur on preferred timescales. The atmospheric stochastic forcing may,

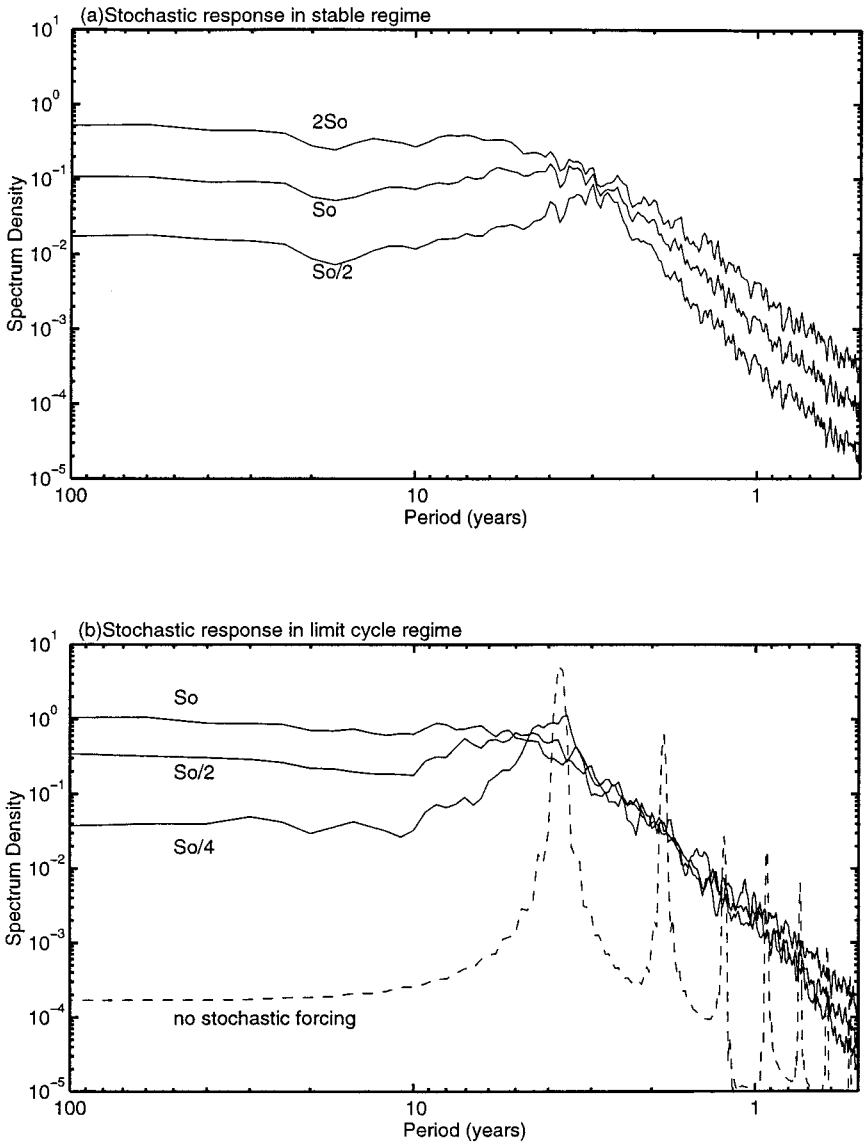

FIG. 8. Dependence of the response spectrum on the strength of a white noise forcing: (a) in the stable regime (point A in Fig. 2) and (b) in the limit cycle regime (point B in Fig. 2). The strength of the white noise is measured by its standard deviation $S_0 = 1.17$ m s^{-1}. The dashed curve in (b) is the spectrum of nonlinear oscillation without stochastic forcing.

therefore, display specific temporal structure or spectral characteristics. These are colored noises. One way to distinguish the types of noise is based on their spectral characteristics. Our numerical experiments have demonstrated that, regardless of the differences in the individual realizations of a type of stochastic forcing, as long as the spectrum of the forcing is the same (or very close), the resultant response spectrum of the ENSO system is practically the same. This lays a foundation for an objective classification of different stochastic forcing.

Four types of stochastic forcing were designed to mimic the statistical features of the tropical atmospheric disturbances: red, white, intraseasonal noise, and synoptic noise. The method of constructing these noises is described in appendix B. The types of colored noise are essentially band-limited white noise. The spectra for each type of forcing are plotted in Fig. 9a. The total energy level of noise can be measured by the standard deviation of the noise time series. The red and white noises in Fig. 9a have the same standard deviation (0.59 m s^{-1}), whereas the intraseasonal and synoptic noises have a much larger standard deviation of about 4 m s^{-1}. As will be seen shortly, even with a much higher energy level, the colored noises are less effective in exciting low-frequency oscillation of the coupled system.

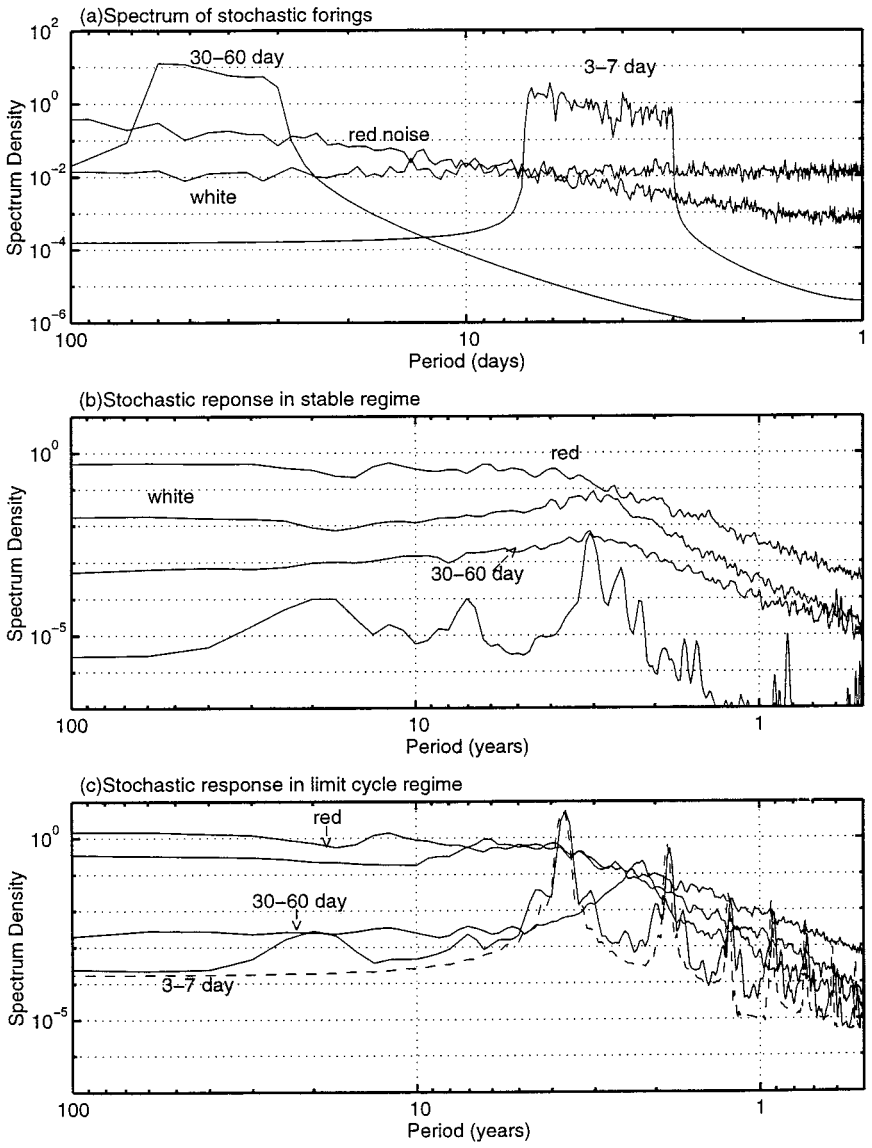

FIG. 9. (a) Characteristic spectra of four types of stochastic forcing: white, red, intraseasonal, and synoptic noises. The standard deviations of stochastic forcing are 0.59 m s^{-1} for white noise and red noise, 3.8 m s^{-1} for intraseasonal noise, and 4.1 m s^{-1} for synoptic noise, respectively. (b) Response spectrum of the ENSO system (2.1) to the four types of stochastic forcing in the stable regime (point A in Fig. 2). (c) The same as in (b) except for the limit cycle regime (point B in Fig. 2). The dashed curve shows the spectrum of the limit cycle oscillation without stochastic forcing.

Figures 9b and 9c compare stochastic responses of the same ENSO system to different types of stochastic forcing. In the stable regime (Fig. 9b), the red noise is most effective in exciting stochastic resonance and raising energy levels at all frequencies, whereas the synoptic noise is least effective. The resonant frequency, however, does not sensitively depend on the type of the forcing. Major spectral peaks (or binding of the spectrum) occur around 3 yr. In the unstable limit cycle regime (Fig. 9c), the stochastic response also sensitively depends on the types of forcing. The synoptic noise hardly changes the intrinsic nonlinear oscillation. The intraseasonal noise, however, alters intrinsic oscillation by shifting the dominant period from about 3 yr to 2 yr and by broadening the spectral peak thereby increasing irregularities. Again, the red noise is most effective in changing the overall characteristics of the intrinsic nonlinear oscillation.

The change of intrinsic oscillation period by intraseasonal noise is an interesting finding. Because the

intensity of the Madden–Julian oscillation (Madden and Julian 1972) varies seasonally—being strong in northern winter and weak in northern summer (Madden 1986, Wang and Rui 1990), we constructed an annually modulated intraseasonal noise that simulates the monsoon modulation of the intraseasonal oscillation. The results revealed that the monsoon's modulation to intraseasonal oscillation favors a stronger interannual oscillation when the system is unstable.

6. Effects of the basic-state variation and the nonlinearity of the ENSO system

a. Effects of the annual variation of the basic state

As mentioned in section 3, the annual variation of the basic state plays a critical role in ENSO evolution. On the one hand, it tends to lock the evolution of ENSO to the annual cycle. On the other hand, it is a source of deterministic chaos. In this section we examine the role of the basic-state annual cycle in the stochastic responses of the ENSO system. The parameters describing the basic-state annual cycle are the same as used in WF96.

Figure 10 compares the stochastic response spectra of the ENSO system in the absence of versus in the presence of a basic-state annual cycle for three different values of the air–sea coupling coefficient α. The forcing used is an intraseasonal noise. The differences in the response spectra for the cases with and without a basic-state annual cycle are insignificant when the system is in a highly stable or highly unstable regime, that is, α is sufficiently far away from the bifurcation value α_0 for the annual mean state (Figs. 10a,c). However, when $\alpha = \alpha_0$, the annual variation of the basic state renders the stochastic response a considerably stronger and less irregular oscillation than that without the annual cycle (Fig. 10b). The oscillation period is also reduced to about 2 yr. In general, the stochastic oscillation in the presence of basic-state annual cycle resembles a shortened limit cycle oscillation. This implies that an intraseasonal noise forcing working together with the basic-state annual variation may effectively excite a finite-amplitude interannual oscillation in a marginally stable regime. In addition, the response shows a sharp peak at the annual timescale, reflecting the impact of the basic-state annual variation on the interannual oscillation of the coupled system.

The phase locking of the model's ENSO to the annual cycle in the presence of the stochastic forcing is not necessarily weaker than that without stochastic forcing. The degree of phase locking to the annual cycle appears to depend on how the stochastic forcing alters the intrinsic oscillation period. When the stochastic forcing shortens the oscillation period, the degree of ENSO phase locking to the annual cycle increases.

b. Effects of the nonlinearity of the ENSO system

To explore the sensitivity of the stochastic response to the degree of nonlinearity in the ENSO system, we designed a hierarchy of stochastic dynamic models with a progressively reduced degree of nonlinearity: (i) a full nonlinear model, (2.1); (ii) a quadratic nonlinear model obtained by removing all cubic nonlinear damping terms; and (iii) a linear model. In order to facilitate comparison, the stochastic forcing is kept the same (a white noise) and the basic-state annual cycle is excluded.

In the stable regime, the linear model exhibits the strongest stochastic resonance and shortest primary oscillation period (Fig. 11a). With an increasing degree of nonlinearity the amplitude of the stochastic resonant oscillation decreases and the oscillation period increases.

In the limit cycle regime, only nonlinear models can produce finite-amplitude irregular oscillations. Compared to the nonstochastic model, the white noise forcing tends to shorten the period of limit cycle oscillation (Fig. 11b). The reduction of oscillation period occurs primarily in the system with the quadratic nonlinearity, whereas the cubic nonlinearity has little effect on the oscillation period. However, the cubic nonlinearity results in a considerable reduction of the energy peak on the ENSO timescale as expected from its damping effects.

7. Summary and discussion

Observed interannual variations in SST, the surface winds, and sea level pressure, and the thermocline displacement in the tropical Pacific show that, to a good lowest-order approximation, the dominant mode of ENSO represents a basinwide east–west standing oscillation. The temporal evolution of the standing ENSO mode can be described by a stochastically forced nonlinear dynamic system, Eq. (2.1). This system consists of a pair of a second-order stochastic differential equations with periodic coefficients representing the basic-state annual cycle.

The physics of the stochastic dynamic model for ENSO (the ENSO system) is highlighted by the schematic diagram shown in Fig. 12. Its essential components include the deterministic dynamics of the coupled ocean–atmosphere system, the external stochastic forcing due primarily to atmospheric high-frequency wind fluctuations, and the impact of the annual variation of the basic state. The deterministic dynamics of the ENSO system exhibits three dynamical regimes (the stable, the limit cycle, and the multiequilibrium), depending on the basic state, the air–sea coupling coefficient α, and the thermocline effect parameter μ. For a fixed $\mu > \mu_0$, the air–sea coupling coefficient α may be viewed as a bifurcation parameter controlling the dynamical regimes of the system (Fig. 2).

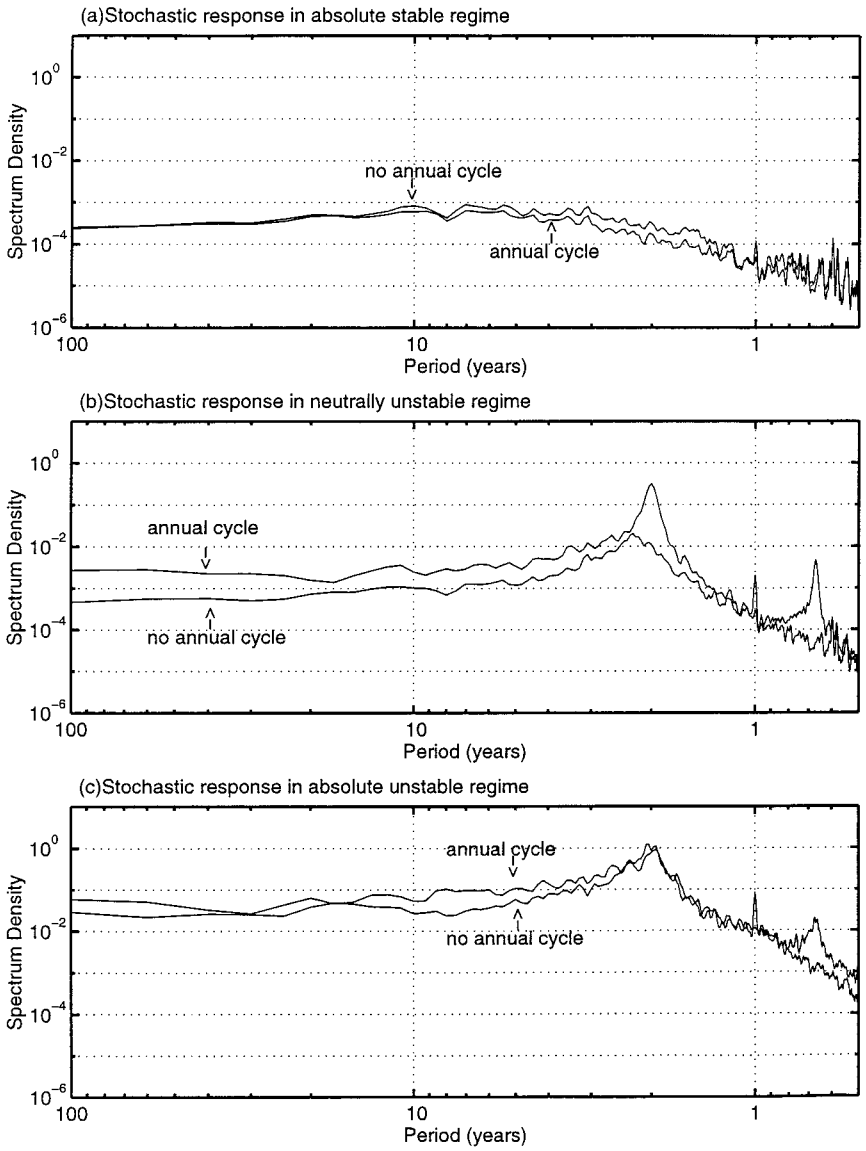

FIG. 10. Comparison of the response spectrum of the ENSO system (2.1) to an intraseasonal stochastic forcing with and without the basic-state annual cycle for the air–sea coupling coefficient $\alpha = 0.05$ (highly stable) (a), $\alpha = \alpha_0$ (marginally stable) (b), and $\alpha = 0.23$ (highly unstable) (c). The thermocline effect parameter $\mu = 1.8$.

The model-simulated interannual oscillations (such as those shown in Figs. 5a,b) capture qualitatively some rudimentary features of observed ENSO, which include (i) a broad spectral peak on the interannual timescale (about 2–7 yr); (ii) a phase locking to the annual cycle; and (iii) irregularities in the oscillation, which appear to consist of both a low-order chaos and high-dimensional randomness, although the detailed forms of evolution in each cycle appear to differ from those of the observed realizations. In this sense, the temporal structure of the model ENSO is realistic.

The nature of the model irregular interannual oscillation critically depends on the nonlinear dynamic regimes of the ENSO system. In the stable regime, the coupled deterministic dynamics cannot sustain oscillations. However, the stochastic forcing can excite and sustain irregular oscillations by stimulating a resonant response of the system (Fig. 5a). The resonant oscillation has a periodicity close to that of the intrinsic decaying oscillation found in the absence of stochastic forcing.

In the limit cycle regime, the unforced deterministic dynamics sustains the intrinsic nonlinear oscillation (stable limit cycle) (Fig. 3a). The stochastic forcing makes the phase orbits scatter around the deterministic limit cycle trajectory in a phase space. In particular, the

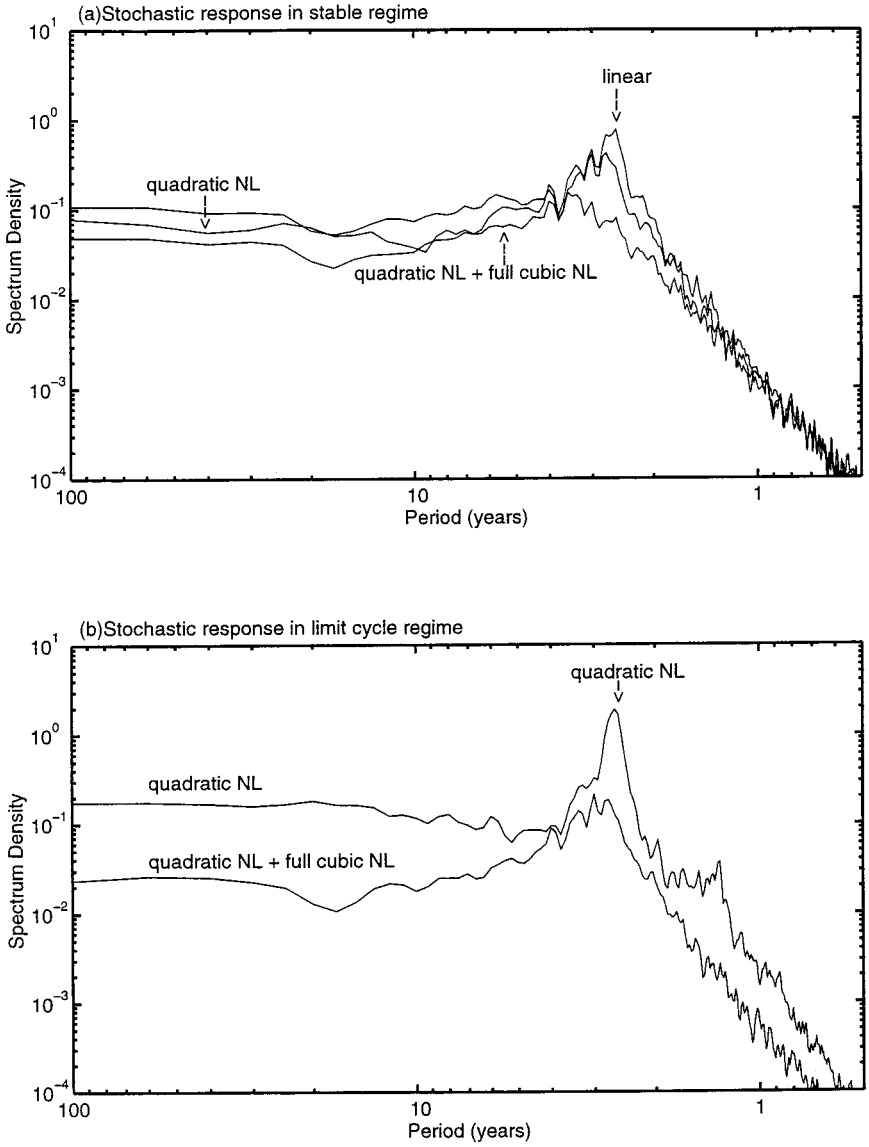

FIG. 11. Comparison of the response spectrum among a linear and a hierarchy of nonlinear systems to a white noise forcing in (a) the stable regime (point A in Fig. 2) and (b) the limit cycle regime.

state of the coupled system tends to densely populate around two preferred extreme states where the tendency of the nonlinear dynamics is weakest (Fig. 6). The resulting stochastic oscillation exhibits high-dimension irregularities, and occasionally prolonged warm or cold episodes (Fig. 5b).

In the multiequilibrium regime, the ENSO system possesses two *stable* equilibrium states—a warm and a cold state and two *unstable* saddles in addition to the unstable climatological basic state (Fig. 7). The deterministic dynamics establishes the two basins of attraction for the warm and cold steady states and the depth of the ''potential wells'' associated with the two attractors. Any perturbation away from the climatological basic state would lead to one of the equilibrium states, depending in which attraction basin the initial perturbation lies. The stochastic forcing may produce motions of sufficient intensity so that the phase of the system may escape from one attraction basin to the other. As a result, the coupled system switches randomly between the two equilibrium states, resulting in an irregular oscillation on interannual or longer timescales. The period of the oscillation depends on the strength of the forcing and the parameters governing the deterministic dynamics.

The stochastic response of the nonlinear ENSO system also depends critically on the properties of the stochastic forcing. For the resonant oscillation, an increase

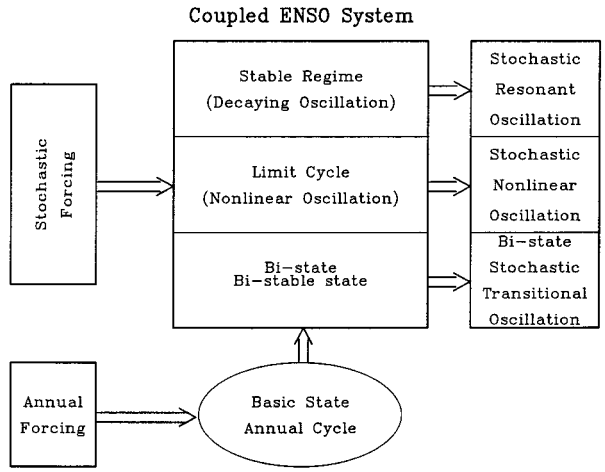

FIG. 12. Schematic diagram showing the essential components and the response of the stochastically forced ENSO dynamic system.

in the intensity of the white noise forcing yields an increased amplitude and prolonged period (Fig. 8a). For the nonlinear oscillation, increasing white noise intensity tends to reduce the amplitude and increases the period and irregularity of the oscillation (Fig. 8b). A sufficiently strong stochastic forcing, however, can destroy the intrinsic nonlinear oscillation or the resonant oscillation, leading to a Markovain process (Fig. 8). The red noise is most effective whereas the synoptic (3–7 days) noise is least effective in exciting resonance and in altering the characteristics of the intrinsic oscillation. Intraseasonal noise can substantially modify the intrinsic nonlinear oscillation by reducing the oscillation period, favoring biennial oscillation (Fig. 9c), especially when the intraseasonal forcing is modulated by monsoons (annual cycle).

The basic-state annual cycle makes the intrinsic deterministic nonlinear oscillation chaotic (Fig. 3b). In the presence of stochastic forcing, the annual variation of the basic state does not alter the stochastic response significantly if the ENSO system is far away from the marginally stable regime. However, in the marginally stable regime, the annual cycle of the basic state tends to enhance the resonant oscillation and to reduce the oscillation period considerably (Fig. 10b).

Increasing the nonlinearity of the ENSO system tends to weaken the resonant response. In other words, a linear ENSO system exhibits the strongest stochastic resonance and may most effectively shorten the oscillation period (Fig. 11a). The stochastic resonance of the linearized ENSO system then is the counterpart in this model of the statistical ENSO models derived from observations (Penland and Matrosova 1994; Penland and Sardeshmukh 1995; Penland 1996).

The model results suggest that the observed irregular ENSO cycles may arise from different origins. The coupled instability and nonlinear dynamics of the coupled ocean–atmosphere system may be a dominant cause in the intermediate coupled models such as Zebiak and Cane (1987). The stochastic forcing in this case would further modify the system's intrinsic oscillation by altering the dominant oscillation period and adding high-dimension irregularities. The stochastic resonance is another possible cause, in particular in the coupled GCMs (Chang et al. 1996). In this case, the climatological mean state is stable and the stochastic forcing sustains irregular ENSO cycles through the stochastic resonance. The last possibility is associated with stochastic transition or switching between a warm and a cold stable equilibrium state. The data analysis by Penland and Sardeshmukh (1995) does not appear to support this bimodal behavior, although Wyrtki (1982) strongly emphasized the bimodal nature of the ENSO. We speculate that in reality and in the coupled ocean–atmospheric models, the interannual oscillations of the tropical climate system may involve multimechanisms and that different mechanisms may be at work at different phases of the oscillations. This hypothesis may explain why the ENSO episodes evolve with great varieties and why the models with considerably different dynamics are all capable of making meaningful predictions at various phases of ENSO cycles, but often with a large discrepancy in the forecasts at the same phases of ENSO.

The stochastic forcing in this model has been projected to the spatial structure of the standing ENSO mode. The intraseasonal noise could have larger amplitude than other types of noise because the large-scale spatial structure of the atmospheric intraseasonal oscillation in the tropical Pacific bears similarities to that of ENSO (e.g., Madden and Julian 1972; Lau and Chan 1988). The intraseasonal noise is shown to be much more effective than synoptic noise in stimulating stochastic resonance, in altering the characteristics of self-sustained oscillations, and especially in reducing the oscillation period, favoring biennial oscillation. These effects are significantly enhanced when the intraseasonal forcing is modulated by monsoons and in the presence of the annual variation of the basic state. These results imply that the atmospheric intraseasonal oscillation may play a much more active role than synoptic disturbances in ENSO evolution, and the monsoons may affect ENSO through modulation of the intraseasonal forcing, enhancing the biennial component of ENSO.

The stochastic dynamic model considered here treats the coupled ENSO mode as an east–west standing oscillation. Although this crucial approximation describes the most important empirical orthogonal function (EOF) of ENSO and leads to advantageous theoretical simplification, it does not describe features of the ENSO mode in the transitional phases, for example, the second EOF. The flaws associated with this simplification were discussed in some detail in WF96. The majority of these deficiencies can be eliminated by increasing the degree of freedom of the system at the price of the loss of analytical clarity. In view of the model's limitation, the conclusions drawn here need to be further examined

using more realistic coupled models. In those models the spatial structure of the stochastic forcing is an inherent component of the stochastic dynamics. In the present work, we have primarily focused on the dynamics for which the climatological mean state was used as a basic state. In the presence of the time-dependent basic state, especially the annual cycle of the basic state, complexity arises from the competition between the coupled instability of the center (the mean state) and that due to parametric forcing via basic-state variation. This issue is currently under investigation.

Acknowledgments. This study has been supported by NOAA GOALS and PACS programs and by Marine Meteorology Program of the Office of Naval Research. Albert Barcilon greatly acknowledges partial support by AFOSR F49620-96-1-0172. He also gratefully acknowledges many insightful discussions with Drs. C. Penland and K. Weickmann during his summer visit to the Climate Diagnostic Center of NOAA and CIRES/University of Colorado. We thank Mr. R. Wu for preparing Fig. 1.

APPENDIX A

Derivation of the Stochastic Dynamic Model for ENSO

To focus on interannual variations, Zebiak and Cane (1987) treated ENSO as a low-frequency departure from its climatological mean (annual cycle) and established an anomaly coupled model. The model consists of an active upper ocean with a mean depth H that overlays an inert deep ocean with the thermocline as their interface. To describe the SST variations, a frictional mixed layer with constant depth (H_1) is embedded in the active upper ocean.

The SST variation in the equatorial eastern Pacific is primarily associated with the upwelling process. We assume that an anomalous downwelling (upwelling) suppresses (enhances) the mean upwelling and induces anomalous warming (cooling). The mixed layer temperature or SST is therefore governed by the following vertically integrated thermodynamic equation:

$$\frac{\partial T}{\partial t} + \frac{w}{H_1}[\overline{T} - \overline{T}_e + T - T_e] + \frac{\overline{w}}{H_1}(T - T_e) = -\alpha_s T, \tag{A1a}$$

where overbars denote basic-state quantities, whereas the variables without an overbar represent anomalies; α_s is a Newtonian cooling coefficient that represents all processes that relax the SST back to its climatology (Neelin et al. 1994); T_e denotes the temperature of subsurface water that upwells into the mixed layer. Following Battisti and Hirst (1989), a simple parameterization of T_e in terms of thermocline depth anomaly h follows:

$$T_e = \mu_* h, \tag{A1b}$$

where the coefficient μ_* measures the influence of thermocline fluctuations on the SST. The upwelling w is generated primarily by the Ekman divergence in the mixed layer, which can be determined by the momentum balance among wind stress, Coriolis, and frictional forces. Assume the Ekman flow to be confined to the mixed layer. It can be shown that the equatorial upwelling is approximately given by (WF96)

$$w \approx -H_2 \frac{l\beta U_a}{r_s^2} u_a, \tag{A1c}$$

where $H_2 = H - H_1$, β is the meridional gradient of Coriolis parameter, u_a denotes surface zonal wind, U_a is a characteristic scale for surface wind speed, $l = \rho_a C_D/(\rho_0 H)$ is a wind stress coefficient, where ρ_a and ρ_o are the densities of the surface air and seawater, respectively, C_D is the drag coefficient, and r_s is the Rayleigh friction coefficient in the oceanic mixed layer. Equation (A1c) implies that an equatorial anomalous westerly induces anomalous convergence and downwelling.

The governing equation for the thermocline depth anomaly may be written as

$$y^2 \frac{\partial h}{\partial t} + \frac{g'H}{\beta^2}\frac{\partial}{\partial t}\left(\frac{2}{y}\frac{\partial h}{\partial y} - \frac{\partial^2 h}{\partial y^2}\right) - \frac{g'H}{\beta}\frac{\partial h}{\partial x} = \frac{lU_a H}{\beta}\left(y\frac{\partial u_a}{\partial y} - u_a\right), \tag{A2}$$

which describes the upper active ocean dynamics forced by zonal wind stress and its associated curl. This equation was derived from a linear, reduced gravity model on the equatorial β plane for the upper ocean with the long-wave approximation (WF96). In the absence of the wind forcing, Eq. (A2) describes free equatorial Kelvin waves and a family of long Rossby waves.

To obtain the surface winds, a simplified Lindzen–Nigam (1987) model is used in which the boundary layer winds are taken to be nondivergent. The distortion of *zonal* winds arising from the nondivergent approximation is small over the equatorial wave guide where the ocean dynamics matters. The resultant surface zonal wind near the equator is given by the following diagnostic equation (WF96):

$$u_a = \frac{dR}{r_a^2 + \beta^2 y^2}\left(r_a \frac{\partial T}{\partial x} + \beta y \frac{\partial T}{\partial y}\right) + u_a^s, \tag{A3}$$

where r_a is the Rayleigh frictional coefficient, d a nondimensional depth of the atmospheric boundary layer, R the gas constant, and u_a^s the zonal stochastic wind forcing. Near the equator, the principal zonal wind forcing is simply proportional to the zonal SST gradient.

The coupled tropical ocean and atmosphere system is thus governed by two prognostic equations: one for SST, Eq. (A1), and the other for thermocline depth anomalies, Eq. (A2). The two equations form a closed

system with the diagnostic relations for zonal wind (A3). The simple system of governing equations, (A1)–(A3), is referred to as *the ENSO system.* It can be extended to a more general formulation by including horizontal temperature advection process (WF96).

The present model involves a number of geophysical and geometrical parameters, listed in Table 1. To nondimensionalize the ENSO system, one may use L_x, L_y, τ, θ, and H_1 to scale x, y, t, T, and h, respectively, where $L_x = L/2$, $\tau = r_s^2 LH/(2\beta H_2 C_0^2)$, and $\theta = (r_a C_0/dR)(L/2l)$. Here L is the ocean basin width, C_0 is the oceanic Kelvin wave speed. The above scaling leads to the following nondimensional SST and thermocline-depth equations:

$$\frac{\partial T'}{\partial t'} = \frac{\partial T'}{\partial x'}(\Delta\overline{T}'_z + T' - \mu' h') + \overline{T}'_x(T' - \mu' h') - \alpha'_s T' + u_a^{s'}(\Delta\overline{T}'_z + T - \mu' h'), \tag{A4}$$

$$\delta\frac{\partial}{\partial t}\left[y'^2 h' + \epsilon\left(\frac{2}{y'}\frac{\partial h'}{\partial y'} - \frac{\partial^2 h'}{\partial y'^2}\right)\right] - \frac{\partial h'}{\partial x'} = -\frac{\partial T'}{\partial x'} + y\frac{\partial u_a^{s'}}{\partial y} - u_a^{s'}, \tag{A5}$$

where prime denotes nondimensional quantities, the basic-state parameters $\Delta\overline{T}'_z = (\overline{T} - \overline{T}_e)/\theta$, $\overline{T}'_x = (L/2\theta)\partial\overline{T}/\partial x$, $\alpha'_s = \alpha_s\tau$, $u_a^{s'} = u_a^s(2\tau/L)$, and nondimensional parameters are

$$\mu = \frac{\mu_* H_1}{\theta}, \tag{A6a}$$

$$\epsilon = \left(\frac{L_0}{L_y}\right)^4, \tag{A6b}$$

$$\delta = \frac{H_2}{H}\left(\frac{L_y}{L_{r_s}}\right)^2, \tag{A6c}$$

where L_o is the oceanic Rossby radius of deformation and $L_{r_s} = r_s/\beta$ is a meridional scale over which Ekman transport spreads SST anomalies on the ENSO development timescale.

The observed SST and the 20°C isotherm depth anomalies exhibit a spatial pattern that is nearly symmetrical and trapped at the equator and resembles, to the lowest order approximation, an east–west seesaw oscillation (Fig. 1). By considering only the largest scale standing basin mode and by using Lorenz's (1963) approach, this characteristic spatial structure allows us to introduce a crucial spatial truncation. Assume that the coupled basin mode solution of the ENSO system and the zonal stochastic wind forcing, u_a^s, have the form $\tilde{T}(x', t')$ [or $\tilde{h}(x', t')$] and $\tilde{u}_a^s(x', t')$ times the lowest-order parabolic cylindrical function $D_0(y') = e^{-1'^2/2}$ and that the mean state is invariant in the meridional direction. Substituting the assumed solutions into Eqs. (A4) and (A5) and projecting the resultant equations onto the lowest meridional mode yield a set of partial differential equations in x and t, for which the simplest spatial finite difference form may be obtained by considering two equal-sized boxes (Battisti and Hirst 1989) representing the eastern and western Pacific, respectively. Since the SST variation in the western Pacific is much smaller than that in the eastern Pacific, we neglect the SST anomalies in the western box. Assuming that thermocline depth anomaly is precisely out of phase between the two boxes and taking the node point of the standing oscillation at the center of the basin as the origin, one finally ends up with the following ENSO system:

$$\frac{dT}{dt} = (\Delta\overline{T}'_z + \Delta\overline{T}'_x - \alpha'_s)T - \mu\overline{T}'_x h + \sqrt{\frac{2}{3}}T(T - \mu h) + \Delta\overline{T}'_z u^s, \tag{A7}$$

$$\frac{dh}{dt} = b(2h - T) - 3bu^s, \tag{A8a}$$

where T and h denote, respectively, anomalous SST and thermocline depth averaged over the equatorial eastern Pacific, u^s represents stochastic zonal wind forcing, and

$$b = \frac{2}{\delta(1 - 3\epsilon)}. \tag{A8b}$$

Introducing an air–sea coupling coefficient

$$\alpha = (L_0/L_y)^2, \tag{A9a}$$

one can rewrite

$$b = \frac{2\alpha}{p(1 - 3\alpha^2)}, \tag{A9b}$$

where $p = (H_2/H)(L_0/L_{r_s})^2$ is a basic-state parameter.

APPENDIX B

Construction of Stochastic Wind Forcing

Three types of stochastic zonal wind forcing—that is, white noise, red noise, and band-limited white (intraseasonal or synoptic) noise, are used in the present study. The white noise is generated by choice of random numbers with a uniform distribution in $[-a, a]$. It can be shown that the standard deviation of the generated white noise, $s = a/\sqrt{3}$. The red noise is generated using the first order autoregression [AR(1)] model. The band-limited white noise is generated using

$$u^s = \sum_{i=1}^{N} A_i \cos(\omega_i t + \phi_i), \tag{B1}$$

where A_i, ω_i, and ϕ_i are all chosen randomly with a uniform distribution over $(0, A)$, $[\omega_a, \omega_b]$, and $[0, 2\pi]$, respectively. In this paper, $N = 400$ is used to ensure that the spectrum of any realization of the colored noise

is nearly the same. Sensitivity tests indicate that 400 harmonics produce a spectrum that is sufficiently close to those obtained using more than 400 harmonics. For an intraseasonal noise, $\omega_a = (2\pi/30)$ (1 day)$^{-1}$, and $\omega_b = (2\pi/60)$ (1 day)$^{-1}$. For a 3–7-day synoptic noise, $\omega_a = (2\pi/3)$ (1 day)$^{-1}$, and $\omega_b = (2\pi/7)$ (1 day)$^{-1}$.

REFERENCES

Battisti, D. S., and A. C. Hirst, 1989: Interannual variability in the tropical atmosphere–ocean system: Influence of the basic state and ocean geometry. *J. Atmos. Sci.,* **46,** 1678–1712.

Bjerknes, J., 1969: Atmospheric teleconnections from the equatorial Pacific. *Mon. Wea. Rev.,* **97,** 163–172.

Blanke, B., J. D. Neelin, and D. Gutzler, 1997: Estimating the effect of stochastic wind stress forcing on ENSO irregularity. *J. Climate,* **10,** 1473–1486.

Cane, M. A., and D. W. Moore, 1981: A note on low-frequency equatorial basin modes. *J. Phys. Oceanogr.,* **11,** 1578–1584.

——, M, Münnich, and S. E. Zebiak, 1990: A study of self-excited oscillations of the tropical ocean–atmosphere system. Part I: Linear analysis. *J. Atmos. Sci.,* **47,** 1562–1577.

Chang, P., B. Wang, T. Li, and L. Ji, 1994: Interactions between the seasonal cycle and ENSO-frequency entrainment and chaos in a coupled ocean–atmosphere model. *Geophys. Res. Lett.,* **21,** 2817–2820.

——, L. Ji, B. Wang, and T. Li, 1995: On the interactions between the seasonal cycle and El-Niño–Southern Oscillation in an intermediate coupled ocean–atmosphere model. *J. Atmos. Sci.,* **52,** 2353–2372.

——, ——, H. Li., and M. Flugel, 1996: Chaotic dynamics versus stochastic processes in El Niño–Southern Oscillation in coupled ocean–atmosphere models. *Physica D,* **98,** 301–320.

Eckert, C., and M. Latif, 1997: Predictability of a stochastically forced hybrid coupled model of El Niño. *J. Climate,* **10,** 1488–1504.

Farrell, B., and P. J. Ioannou, 1996: Generalized stability theory. Part I: Autonomous operators. *J. Atmos. Sci.,* **53,** 2025–2040.

Gardiner, C. W., 1983: *Handbook of Stochastic Methods in Physics, Chemistry, and other Natural Sciences.* Springer-Verlag, 442 pp.

Graham, N. E., and W. B. White, 1988: The El Niño cycle: A natural oscillator of the Pacific Ocean–atmosphere system. *Science,* **24,** 1293–1302.

Hirst, A. C., 1986: Unstable and damped equatorial modes in simple coupled ocean–atmosphere models. *J. Atmos. Sci.,* **43,** 606–630.

Ji, M., A. Leetmaa, and J. Derber, 1995: An ocean analysis system for seasonal to interannual climate studies. *Mon. Wea. Rev.,* **123,** 460–481.

Jin, F.-F., J. D. Neelin, and M. Ghil, 1994: El Niño on the devil's staircase: Annual subharmonic steps to chaos. *Science,* **264,** 70–72.

Kirtman, B. P., 1997: Oceanic Rossby waves and the ENSO period in a coupled model. *J. Climate,* **10,** 1690–1704.

Kleeman, R., and S. B. Power, 1994: Limits to predictability in a coupled ocean–atmosphere model due to atmospheric noise. *Tellus,* **46**A, 529–540.

——, and A. M. Moore, 1997: A theory for the limitations of ENSO predictability due to stochastic atmospheric transients. *J. Atmos. Sci.,* **54,** 753–767.

Lau, K. M., 1985: Elements of a stochastic dynamical theory of the long term variability of the El Niño/Southern Oscillation. *J. Atmos. Sci.,* **42,** 1552–1558.

——, and P. H. Chan, 1988: Intraseasonal and interannual variations of tropical convection: A possible link between the 40–50 day oscillation and ENSO? *J. Atmos. Sci.,* **45,** 506–521.

Lindzen, R. S., and S. Nigam, 1987: On the role of sea surface temperature gradients in forcing low level winds and convergence in the tropics. *J. Atmos. Sci.,* **44,** 2418–2436.

Lorenz, E. N., 1963: Deterministic nonperiodic flow. *J. Atmos. Sci.,* **20,** 130–141.

Madden, R. A., 1986: Seasonal variations of the 40–50 day oscillation in the tropics. *J. Atmos. Sci.,* **43,** 3138–3158.

——, and P. R. Julian, 1972: Description of global-scale circulation cells in the tropics with a 40–50 day period. *J. Atmos. Sci.,* **29,** 1109–1123.

McCreary, J., 1983: A model of tropical ocean–atmosphere interaction. *Mon. Wea. Rev.,* **111,** 370–389.

Münnich, M., M. A. Cane, and S. E. Zebiak, 1991: A study of self-excited oscillations of the tropical ocean–atmosphere system. Part II: Nonlinear cases. *J. Atmos. Sci.,* **48,** 1238–1248.

Neelin, J. D., 1991: The slow sea surface temperature mode and the fast wave limit: Analytic theory for tropical interannual oscillations and experiments in a hybrid coupled model. *J. Atmos. Sci.,* **48,** 584–606.

——, M. Latif, and F.-F. Jin, 1994: Dynamics of coupled ocean–atmosphere models: The tropical problem. *Annu. Rev. Fluid Mech.,* **26,** 617–695.

Penland, C., 1996: A stochastic model of the IndoPacific sea surface temperature anomalies. *Physica D,* **98,** 534–558.

——, and L. Matrosova, 1994: A balance condition for stochastic numerical models with application to the El Niño–Southern Oscillation. *J. Climate,* **7,** 1352–1372.

——, and P. D. Sardeshmukh, 1995: The optimal growth of tropical sea surface temperature anomalies. *J. Climate,* **8,** 1999–2024.

Philander, S. G. H., T. Yamagata, and R. C. Pacanowski, 1984: Unstable air–sea interaction in the tropics. *J. Atmos. Sci.,* **41,** 604–613.

——, R. C. Pacanowski, N. C. Lau, and M. J. Nath, 1992: Simulation of ENSO with a global atmospheric GCM coupled to a high-resolution, tropical Pacific ocean GCM. *J. Climate,* **5,** 308–329.

Suarez, M. J., and P. S. Schopf, 1988: A delayed action oscillator for ENSO *J. Atmos. Sci.,* **45,** 3283–3287.

Trenberth, K. E., and D. J. Shea, 1987: On the evolution of the Southern Oscillation. *Mon. Wea. Rev.,* **115,** 3078–3096.

Tziperman, E., L. Stone, M. Cane, and H. Jarosh, 1994: El Niño chaos: Overlapping of resonances between the seasonal cycle and the Pacific Ocean–atmosphere oscillator. *Science,* **264,** 72–74.

——, M. A. Cane, and S. E. Zebiak, 1995: Irregularity and locking to the seasonal cycle in an ENSO-prediction model as explained by the quasi-periodicity route to chaos. *J. Atmos. Sci.,* **52,** 293–306.

Wakata, Y., and E. S. Sarachik, 1991: Unstable coupled atmosphere–ocean basin modes in the presence of a spatially varying basic state. *J. Atmos. Sci.,* **48,** 2060–2077.

Wang, B., and H. Rui, 1990: Synoptic climatology of transient tropical intraseasonal convection anomalies: 1975–1985. *Meteor. Atmos. Phys.,* **44,** 43–61.

——, and Z. Fang, 1996: Chaotic oscillation of tropical climate: A dynamic system theory for ENSO. *J. Atmos. Sci.,* **53,** 2786–2802.

Wyrtki, K., 1982: The southern oscillation, ocean–atmosphere interaction and El Niño. *Mar. Technol. Soc. J.,* **16,** 3–10.

Zebiak, S. E., and M. A. Cane, 1987: A model El Niño–Southern Oscillation. *Mon. Wea. Rev.,* **115,** 2262–2278.